Carbon 167 (2020) 816–825

Contents lists available at ScienceDirect

Carbon

journal homepage: www.elsevier.com/locate/carbon

Role of anions on electrochemical exfoliation of graphite into graphene in aqueous acids

Hoyoung Lee [a], Ji Il Choi [b], Jinho Park [a], Seung Soon Jang [b, *], Seung Woo Lee [a, **]

[a] George W. Woodruff School of Mechanical Engineering, Georgia Institute of Technology, Atlanta, GA, 30332, USA
[b] Computational NanoBio Technology Laboratory, School of Materials Science and Engineering, Georgia Institute of Technology, Atlanta, GA, 30332, USA

ARTICLE INFO

Article history:
Received 23 April 2020
Received in revised form
14 June 2020
Accepted 15 June 2020
Available online 19 June 2020

Keywords:
Graphite
Electrochemical exfoliation
Graphene
Anions
Binding energy

ABSTRACT

Anodic electrochemical exfoliation of graphite is one of the promising methods for the fast production of graphene with moderate quality at low cost. Sulfate-containing aqueous solutions have been identified as the most efficient electrolyte condition for anionic exfoliation process of graphite into graphene. However, the origin of the high exfoliation efficiency of sulfate-containing electrolytes remains unanswered. In this study, we study the role of anions in anodic exfoliation of graphite by comparing different dilute acid systems (sulfuric, nitric, phosphoric, and hydrochloric acids). Using the combination of in-situ mass spectrometer, cyclic voltammetry, and density functional theory computation modeling, we reveal that only the sulfate anions allows reversible intercalation behavior upon cycling voltammetry cycles, probably due to the highest repulsive binding energy between graphene sheets compared to those of other anions. Therefore, the easy access of sulfate anion into the graphite layer facilitates the diffusion of water molecules into the bulk of the graphite during the anodic process, and the subsequent water oxidation enables efficient exfoliation of graphite into graphene. These results highlight the importance of understanding the interactions between electrolyte ion and graphite for the electrochemical manufacturing of graphene.

1. Introduction

Graphene [1], a single layer of carbon atoms bonded in a honeycomb structure, has attracted significant attention from many researchers due to its exceptional electrical [2,3], mechanical [4,5], chemical [6], thermal [7], and optical [8] properties. Such intriguing properties have led to its potential applications in composite materials [9–15], electronic devices [8,16–18], and energy storage and conversion devices [19–24]. To employ graphene for these applications, many fabrication approaches have been attempted to produce large-scale, high-quality graphene in cost-effective ways. High-quality, wafer-scale graphene can be fabricated by bottom-up processes, such as chemical vapor deposition (CVD) [25,26] or epitaxial growth on SiC [27], for high-end electronic applications. However, the fabrication of graphene on the substrate is impractical for large-scale applications, such as composite materials or energy devices, due to its high cost and slow production rate.

Top-down approach, exfoliation of earth-abundant mineral graphite, has a great potential to provide scalable, cost-effective production ways of graphene towards large-scale applications [28–34]. Micromechanical exfoliation method was first used to produce single-layer graphene from graphite for mostly research purposes [35], but it is not scalable due to the low-yield and slow production rate. Other exfoliation methods, such as sonochemical liquid-phase exfoliation by extended sonication [36] and intercalation expansion using volatile agents [37], have been attempted to produce high-quality graphene, but the progress on scalability and production rate is still not practical. Solution based chemical exfoliation of graphite based on the Hummers methods, which includes the oxidation of graphite with strong acids and oxidants, provides a scalable route to produce graphene oxide (GO) [38,39]. During the strong oxidation process, the sp^2 conjugation carbon network of graphene sheets is oxidized with the formation of various oxygen functional groups, such as hydroxyl, epoxy, carbonyl, and carboxylic acid [40]. The hydrophilic character of these oxygen functional groups on GO enables solution-processable GO dispersions in various solvents, including water. However, the

* Corresponding author.
** Corresponding author.
E-mail addresses: SeungSoon@mse.gatech.edu (S.S. Jang), seung.lee@me.gatech.edu (S.W. Lee).

https://doi.org/10.1016/j.carbon.2020.06.044
0008-6223/

produced GO is almost insulating compared to pristine graphene due to the disruption of long-range conjugation carbon network, requiring subsequent chemical or thermal reduction processes to recover its electrical conductivity [41]. In addition, typical reduction processes involve high-temperature treatment [42] or toxic reducing agents, such as hydrazine [43], sodium borohydride [44], and hydroiodic acid [45].

Electrochemical processing has been applied for the production of nanocarbon materials, such as graphite intercalation compounds (GICs), from the 1960s [46–58]. As graphene has recently emerged as a rising material [5,59–62], this old GIC chemistry has been extended to a new electrochemical method for the exfoliation of graphite into graphene [63–65]. Electrochemical exfoliation process has many advantages over conventional exfoliation methods, including low-cost, simple operation, fast production-rate, and in-situ functionalization [63–79]. Moreover, electromotive force is a more controllable processing parameter compared to other chemical or mechanical driving forces for the exfoliation of graphite [63]. Depending on the applied potentials, graphite is either anodically or cathodically exfoliated interacting with electrolytes, producing different kinds of products such as oxidized graphite [31,69], carbon nanoparticles [72], nanoribbons [72], and low-defect graphene [67,71]. Electrochemical exfoliation process has been studied in various electrolytes, including ionic liquid [11,72], lithium perchlorate in propylene carbonate [33], and aqueous inorganic salt solutions [31,67], and electrolytes with additives [80–82]. Both positive potential (anodic) and negative potential (cathodic) introduce electrolyte ions into the graphite layer structure, weakening van der Waals interactions between graphene sheets. The cathodic exfoliation process in non-aqueous electrolytes has been attempted as a non-oxidative route, producing few-layer graphene with reduced oxygen content [33,79,83,84]. However, using organic solvents is expensive and sensitive to oxygen and moisture, which limits their practical applications. The anodic exfoliation with aqueous inorganic salt solution [31] has been identified as the most efficient condition to produce high-yield graphene. In particular, sulfate-containing electrolytes, such as H_2SO_4, $(NH_4)_2SO_4$ and K_2SO_4, showed exceptional exfoliation efficiency compared to other aqueous electrolyte systems [31,67,69].

The proposed anodic exfoliation process of graphite into graphene in aqueous electrolytes is a complex phenomenon, involving ion intercalation, chemical oxidation, gas evolution, blister formation, mechanical expansion and exfoliation reactions [31,67]. When high electrical potential is applied to the graphite electrode, anodic oxidation of water generates hydroxyl ions (OH-) or oxygen radicals (O•) [67,72,85]. The hydroxylation and oxidation reactions of these ions and radicals at the edges of graphite open up the edge sites, facilitating intercalation by anions, such as SO_4^{2-} [31,67]. During this intercalation process, water molecule co-intercalate to graphitic sheets with the SO_4^{2-} [31,67]. Previous studies suggested that various gaseous species, such as SO_2, O_2, CO, CO_2 can be generated by SO_4^{2-} anion reduction, water oxidation, and carbon corrosion [31,67]. The generated gaseous species can further expand the interlayer distance of graphitic layers, resulting in the separation and production of graphene sheets. The previous study explained that the higher efficiency with sulfate salts may be attributed to the lower standard reduction potential of SO_4^{2-} (+0.20 V) compared to those of other anions (0.96 V for NO_3^-, 1.36 V for Cl^-, and 1.42 V for ClO_4^-) [67]. They hypothesized that the favorable formation of SO_2 gas from SO_4^{2-} compared to other NO or Cl_2 gases is responsible for the effective exfoliation in sulfate-containing solution [67]. However, this hypothesis has not been proven by experiments and it is unclear how the reduction reactions from electrolyte anions can be coupled with other oxidation reactions. In addition, the following questions should be addressed to understand the exfoliation mechanism: 1) What is the role of intercalation reactions of anions into graphite sheets for the exfoliation and corresponding structural change of graphite? 2) How do the other gas evolution reactions, such as O_2 from water oxidation and CO or CO_2 from carbon corrosion, affect the exfoliation process?

Herein, we investigate and compare the electrochemical exfoliation processes of highly oriented pyrolytic graphite (HOPG) in different acidic electrolytes: H_2SO_4, H_3PO_4, HNO_3, and HCl. Detailed physical and chemical characterizations of the graphene product obtained from various electrolytes show that H_2SO_4 has exceptional exfoliation efficiency in producing high-quality graphene. We employ an in-situ mass spectrometer to detect gaseous species during the electrochemical exfoliation of graphite in different electrolyte systems to correlate the water oxidation and carbon corrosion reactions with exfoliation efficiency. Cyclic voltammetry and density functional theory (DFT) computations reveal that sulfate anions can move relatively freely within the graphite lattice compared to other anions. We find that such a unique intercalation property of sulfate anion facilitates the diffusion of more water molecules into the bulk of the graphite during the anodic electrochemical exfoliation process, and the subsequent water oxidation enables efficient exfoliation of graphite into graphene.

2. Experimental section

2.1. Two-electrode electrochemical exfoliation with in-situ gas analysis

Highly oriented pyrolytic graphite (HOPG, mosaic angle = 0.4 ± 0.1°, Alfa Aesar) was cleaved with adhesive tape prior to each experiment. HOPG was used as a working electrode with an area immersed in each electrolyte of 0.2 × 0.5 mm^2. A Pt rod was used as a counter electrode. Electrolytes were prepared by diluting concentrated acids with deionized (DI) water with a resistivity of 18.2 MΩ cm. The concentrated acids, H_2SO_4 (95%), H_3PO_4 (85%), HNO_3 (70%), and HCl (37%), were all purchased from Sigma–Aldrich and used without further purification. For *in-situ* gas analysis, a mass spectrometer (Cirrus 2, MKS Instruments) was connected to the electrochemical cell in series. Ar gas (ultrahigh purity, Airgas) was fed into the electrochemical cell as a carrier gas at a flow rate of 20 mL min^{-1} controlled by a mass flow controller (G-series, MKS Instruments). Prior to the electrochemical exfoliation, the carrier gas was injected for ~30 min until the signal on the gas analyzer was stabilized. A voltage of 10 V with a compliance current of ~1 A was applied by a source meter (2400, Keithley) across the electrodes for 5 min (or 1 min 30 s particularly for the sulfuric acid electrolyte). After the exfoliation, the solid products were collected and washed with DI water/ethanol *via* a vacuum filtration method, while employing Celgard3501 (Celgard) membrane as a filter. After the washing, the solid products were transferred to anhydrous dimethylformamide (DMF, 99.8%, Sigma–Aldrich), followed by sonication for 15 min. The production rate of exfoliated graphene from each acid were calculated based on the layer number statistics, where only graphene flakes of up to four layers were considered. The flow rates of generated gas products were obtained by normalizing partial pressure of each gas (signal on the instrument) against its ionization efficiency and flow rate of the carrier gas.

2.2. Characterizations of the solid products of the electrochemical exfoliation

The morphology of solid products from the exfoliation was investigated by scanning electron microscopy (SEM, SU8230, Hitachi) operated at 0.5 kV at working distance of 5–8 mm, transmission electron microscopy (TEM, HT7700, Hitachi) operated

at 120 kV, and atomic force microscopy (AFM, Icon, Bruker). Chemical analysis of the solid products was performed with X-ray photoelectron spectroscopy (XPS, K-Alpha, Thermo Scientific) with Al Kα source and 15 W X-ray gun power on the spot size of 400 μm. A flood gun was used to offset surface charging. The high-resolution C1s peaks were fitted by the XPSPEAKS 4.1 with background type of Shirley and Gaussian-Lorentzian ratio from 5 to 30%. Raman spectroscopy (Qontor Dispersive Raman Spectrometer, Remishaw) was used to investigate defects of the exfoliation products with 1% of 488 nm laser on the spot size of about 1 μm.

2.3. Cyclic voltammetry

Cyclic voltammetry (CV) was conducted in a three-electrode system connected to a potentiostat/galvanostat (VMP3, BioLogic), while HOPG, Pt rod, and RHE (Gaskatel) were used as working, counter, and reference electrodes, respectively. The three cycles of electric potential sweeps were carried out in a range of 1–2.0 V (vs RHE, particularly 1–2.5 V for the electrolyte of H_3PO_4) at a scan rate of 1 mV/s.

2.4. Density functional theory computations

For the binding energy calculations, graphene surfaces were prepared to accommodate ion molecules, having a dimension of 14.760 Å × 14.760 Å. The solvation effect was not considered in the calculation of binding energy to evaluate the pristine molecular interaction between the graphene and molecular ions. The ionic states of Cl, NO_3, and SO_4 ions in graphene interaction are described in the neutral state as treated in a previous computation study on graphite-cation interaction reaction [86]. Basically, we adopt the same strategy to understand the anion intercalation behavior of graphite and subsequent exfoliation process by calculating the binding energy of various ion species, Cl, NO_3, H_2PO_4, and SO_4. Atomic geometries were optimized by carrying out DFT calculations with a VASP code [87,88]. We performed all the calculations allowing spin polarization within the Perdew-Burke-Ernzerhof parametrization of generalized gradient approximation [89], including van der Waals corrections (DFT-D3) [90]. Valence electronic states were expanded in plane wave basis sets with a 450 eV energy cut off, and the project-augmented wave (PAW) method was used to represent core-valence electron interactions. Monkhorst–Pack sampled [91] 3 × 3 × 1 k-point mesh applied to the calculation of binding energy after checking negligible changes in binding energy at higher k-point mesh.

3. Results and discussion

We carried out electrochemical exfoliation of highly oriented pyrolytic graphite (HOPG) foils in a variety of acidic electrolytes (1 M H_2SO_4, H_3PO_4, HNO_3, and HCl) by applying an electrical voltage of 10 V between two electrodes: the HOPG foil as a working electrode and a platinum rod as a counter electrode, respectively. After conducting the exfoliation for several minutes, the products stripped from the HOPG foils were collected, washed, and then dispersed in dimethylformamide (DMF) (Fig. 1a). Solid products could be collected by conducting the exfoliation in 1 M H_2SO_4, H_3PO_4, and HNO_3, but no solid product was obtained in 1 M HCl. In particular, the exfoliation process with H_2SO_4 showed a significantly higher production rate of 9.55 mg min^{-1} compared to those with H_3PO_4 (0.84 mg min^{-1}) and HNO_3 (1.20 mg min^{-1}). We characterized the morphology of the solid products obtained from the exfoliation process using transmission electron microscopy (TEM), scanning electron microscopy (SEM), and atomic force microscopy (AFM). The TEM images of the products obtained with H_2SO_4 and H_3PO_4 showed well-exfoliated graphene sheets (Fig. 1c and d). On the other hand, the product from the HNO_3 electrolyte is in the form of agglomerated graphene flakes (Fig. 1e). The SEM image further confirmed the aggregated particle morphology of graphene flakes obtained from HNO_3 (Fig. S1). Statistical thickness and size analysis show that the major graphene products are a bilayer graphene for H_2SO_4 and a triplelayer graphene for H_3PO_4 with the size range of 1–5 μm (Fig. S2). On the other hand, a large amount of multilayer graphene products (n > 4) were observed for HNO_3. The representative AFM image and corresponding height profile of the product from H_2SO_4 clearly presented a well-defined graphene structure with a thickness of ~1.5 nm (Fig. 1f). On the other hand, the product from the HNO_3 electrolyte showed a rough profile over a wide thickness range up to 50 nm (Fig. 1g), further confirming the formation of graphene flakes detached from the HOPG foil during the electrochemical process. These observations indicate that the exfoliation process of graphite with H_2SO_4 performs better than other acidic electrolytes in terms of production efficiency and product quality. Additionally, we conducted electrochemical exfoliation of graphite foils under electric potential of 10 V with compliance current of 1 A in 0.1 M H_2SO_4, HNO_3, H_3PO_4, and HCl for 5 min. The electrolyte dependent exfoliation tendency is the same as HOPG, but overall exfoliation process is much faster with graphite foil compared to HOPG (Fig. S3). For example, exfoliation of graphite foil immersed in 0.1 M H_2SO_4 took only about 2 min. To understand this difference, we investigated the morphology of two graphite sources. HOPG shows a flat surface with a large grain size (~hundreds of microns) and has a compactly packed layered structure (Fig. S4a). Graphite foil, on the other hand, shows a much rougher surface with a reduced grain size (~tens of microns), and has a loosely packed structure (Fig. S4b). Therefore, the faster exfoliation rate of graphite foil compared to HOPG can be attributed to the much smaller grain size and larger edge area, which can promote the electrochemical reactions with electrolyte ions.

X-ray photoelectron spectroscopy (XPS) and Raman spectroscopy were conducted to further investigate the structural differences of graphene products in different electrolytes (Fig. 2). First, the detailed surface functional groups of graphene products in 1 M H_2SO_4, H_3PO_4, and HNO_3 were investigated by high-resolution XPS C1s spectra (Fig. 2a–c). The C1s spectra were deconvoluted into sp^2 hybridized carbon at 284.5 eV, sp^3 hybridized carbon at 285.4 eV, C − O bond at 286.1 eV, C = O bond at 286.8, C − OH bond at 287.5 eV, and O = C − OH bond at 288.8 eV [92–95]. All samples contained copious oxygen functional groups, indicating concomitant carbon oxidation during the electrochemical process. A recent study on the electrochemical corrosion of glassy carbon suggested that under acidic conditions, protons can promote the electrophilic addition or substitution of water in a conjugated sp^2 carbon system, leading to the formation of various oxygen functional groups, such as ketones, aldehydes, and carboxylic acid, through subsequent oxidation and condensation steps [96]. This oxidation mechanism well describes the XPS results of the products form the electrochemical exfoliation of HOPG. Interestingly, the product in H_3PO_4 showed a significantly higher atomic ratio of oxygen to carbon (O/C = 0.33) than other samples (0.115 for H_2SO_4 and 0.112 for HNO_3). In addition, the calculated atomic ratios of sp^2 carbon to sp^3 carbon were found to be 2.60 for H_3PO_4, 6.10 for H_2SO_4, and 4.67 for HNO_3. The ratio of sp^2 carbon to sp^3 carbon was estimated by comparing the areas of the sp^2 and sp^3 peaks in the high-resolution XPS C1s spectra [97]. These results indicate that the exfoliated graphene in H_3PO_4 was highly oxidized and defective during the electrochemical process. Raman spectrum of HOPG exhibited characteristic G band (~1580 cm^{-1}) and doublet of 2D band ($2D_1$ at ~2700 cm^{-1} and $2D_2$ at ~2735 cm^{-1}) (Fig. 2d) [98]. After the electrochemical process, all graphene

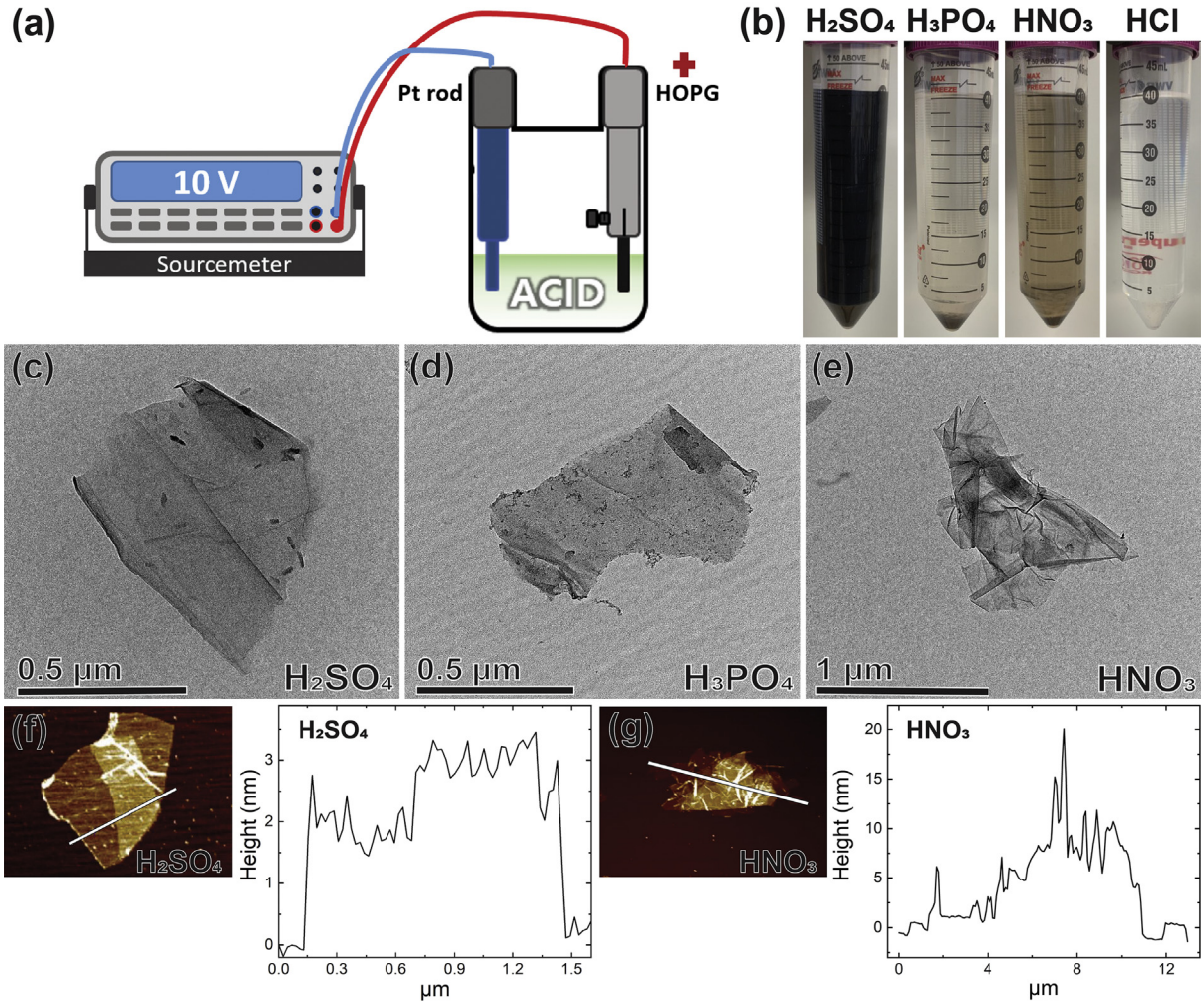

Fig. 1. (a) Schematic illustration of the electrochemical exfoliation set-up. (b) Digital photos of the products obtained by electrochemical exfoliation of HOPG in 1 M H_2SO_4, H_3PO_4, HNO_3, and HCl (from left to right). The products were stored in dimethylformamide (DMF) for three days. TEM images of the products obtained from (c) H_2SO_4 (d) H_3PO_4, and (e) HNO_3. AFM images and the corresponding height profiles of the products obtained through the exfoliation of HOPG in (f) H_2SO_4 and (g) HNO_3.

products showed strong D band around 1354 cm^{-1}, confirming the lattice distortion and defect formation caused by the oxidation process [99,100]. Additionally, the graphene products exhibited a broadened 2D band, which is also a hallmark of disordered carbon [101]. The intensity ratio of the 2D band to the G band (I_{2D}/I_G) is often used as an indicator of the graphitization degree that correlate the impurity concentration in graphene [102]. The I_{2D}/I_G ratios of the graphene products were found to be 0.06 for H_3PO_4, 0.29 for HNO_3 and 0.48 for H_2SO_4. This indicates that the H_2SO_4 electrolyte produced relatively high-quality graphene, while H_3PO_4 exhibited highly defective graphene. Moreover, the characteristics of the slightly shifted G peak (combined with D′) and flat 2D band in H_3PO_4 are similar to the partially reduced graphene oxide (rGO) [103]. Confirming the high degree of oxidation of the graphene product in H_3PO_4. This is also consistent with the XPS results of the highly oxidized structure of graphene in H_3PO_4.

To elucidate the effects of electrolytes on the exfoliation process, we monitored the gaseous products generated from the electrochemical cells during the exfoliation using an *in-situ* gas analysis set-up (Fig. S5). For the *in-situ* gas analysis, the electrochemical cell was purged with Ar gas as a carrier gas at a flow rate of 20 mL min^{-1} and the gaseous products passed through the quadrupole-based mass spectrometer. Fig. 3 shows the gas composition profiles over time during the electrochemical exfoliation process of HOPG with different electrolytes (1 M H_2SO_4, HNO_3, H_3PO_4, and HCl) at an applied voltage of 10 V. When using H_2SO_4 for the electrolyte, O_2 was the major gaseous product, and CO_2 and CO were also detected during the electrochemical exfoliation (Fig. 3a). O_2 can be generated by the oxidation of water molecules, while both CO_2 and CO are due to the oxidation of carbon (HOPG foil). Interestingly, no SO_2 gas was detected during the electrochemical exfoliation in 1 M H_2SO_4. Additionally, we performed water electrolysis with an electrochemical cell consisting of an Au cathode and a Pt anode at 10 V. However, SO_2 was not detected at both the cathode and anode (Fig. S6). The change of electrolyte during the electrochemical exfoliation in H_2SO_4 electrolyte should further be clarified. These results do not support the previous hypothesis that the favorable formation of SO_2 gas from SO_4^{2-} is responsible for the effective exfoliation in sulfate-containing solution [31,67]. Instead, peroxodisulfate anions ($S_2O_8^{2-}$) can be generated by the electrochemical oxidation of sulfate anions under anodic exfoliation conditions [104]. It was found that the O_2 gas generated by water oxidation is the major gas product to irreversibly expand and further exfoliate graphite during the electrochemical process in H_2SO_4. The flow rate of all gaseous products, O_2, CO_2, and CO, increased rapidly up to 2 min 30 s, and then decreased as the remaining HOPG gradually

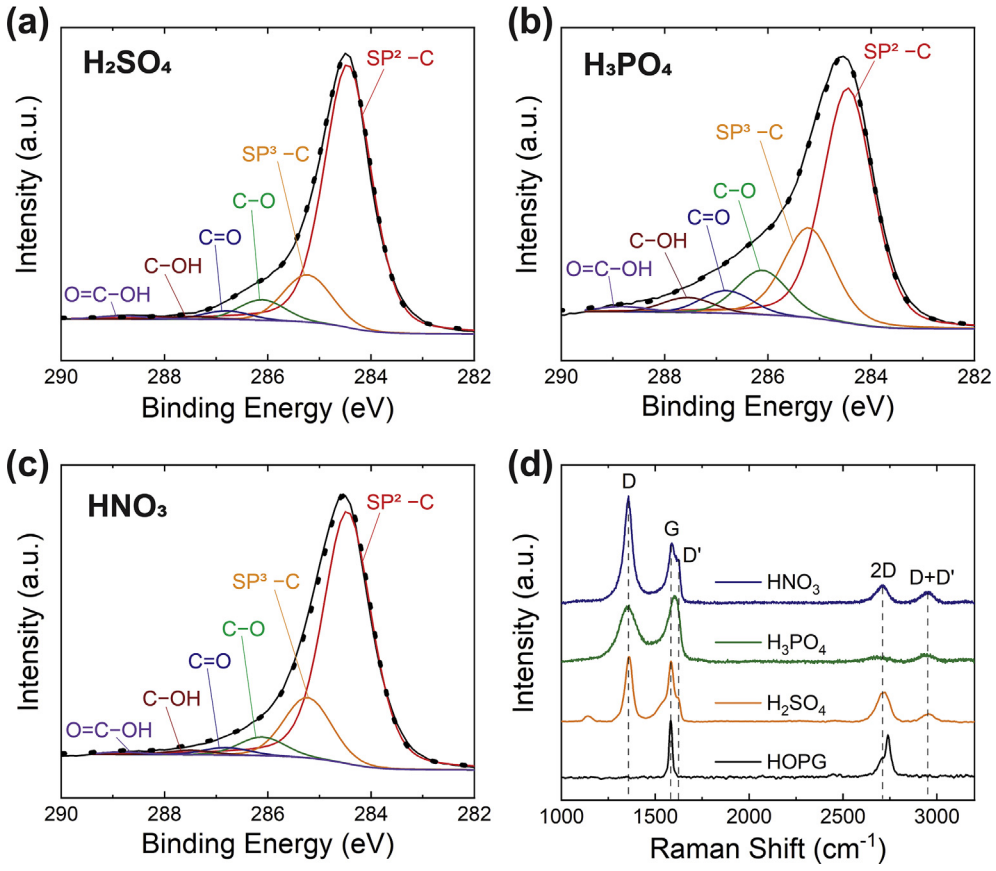

Fig. 2. High-resolution X-ray photoelectron spectroscopy C1s spectrums of electrochemically exfoliated products in (a) H_2SO_4, (b) H_3PO_4, and (c) HNO_3. (d) Raman spectrum of HOPG and electrochemically exfoliated HOPG in different electrolytes. (A colour version of this figure can be viewed online.)

decreased during the exfoliation process. For the H_3PO_4 electrolyte (Fig. 3b), the same gas species (O_2, CO_2, and CO) were detected, but the overall flow rates of gases were relatively lower than those in H_2SO_4. The decreased gas flow rate in H_3PO_4 can be associated with less efficient exfoliation of graphite compared to H_2SO_4. Additionally, for H_3PO_4, the major gaseous product was CO_2, which can be related to the highly oxidized structure of graphene identified by the XPS results. In the case of HNO_3, O_2 gas was mainly produced and relatively small amounts of CO_2 and CO were detected during the exfoliation process (Fig. 3c). A large amount of O_2 gas may be due to multiple reactions. In addition to the water oxidation reaction, NO_3^- anions can be electrochemically oxidized by the following reaction (1) [105]:

$$NO_3^- \rightarrow NO_2 + \frac{1}{2}O_2 + e^- \quad (1)$$

Interestingly, a small amount of NO was also detected in HNO_3 (Fig. S7). The previous study has shown that hydrolysis of the generated NO_2 can produce NO [106]. For HCl, Cl_2 was the major gaseous product during the electrochemical process (Fig. 3d). Unlike other anions in acidic electrolytes, chloride ions were oxidized to generate Cl_2 gas. Therefore, the poor exfoliation efficiency of graphite in HCl can be attributed to the formation of Cl_2 gas before the intercalation reaction (which will be discussed later). The real-time current response (chronoamperometry) and corresponding gas generation were also analyzed during the expansion of HOPG at 2.4 V (vs RHE) (Fig. S8). Relatively high currents are observed in H_2SO_4 and HCl compared to other two electrolytes (HNO_3 and H_3PO_4) which correspond to the amount of gas detected during the expansion. A rapid increase in current for 100 s was observed in H_2SO_4 due to the increase in surface area due to faster expansion compared to other anions.

For an in-depth understanding of the exfoliation process with different electrolytes (1 M H_2SO_4, 1 M H_3PO_4, 1 M HNO_3, and 1 M HCl), we performed cyclic voltammetry (CV) using a three-electrode system (Fig. 4). The HOPG film, the Pt rod, and the reversible hydrogen electrode (RHE) were used as a working, a counter, and a reference electrode, respectively. The first CV scan in 1 M H_2SO_4 showed a large oxidation peak with an onset potential of 1.83 V (vs RHE) that is associated with the intercalation of sulfate anions (SO_4^{2-}) into the graphite layer (Fig. 4a). A followed plateau was observed after 1.88 V (vs RHE), indicating the diffusion of inserted anions through the interlayers of HOPG [107]. A second oxidation wave with an onset potential of 1.96 V (vs RHE) results from a combination of the water oxidation and carbon corrosion reactions, which is supported by the gas bubbles generated around the HOPG (Fig. S9). In the reverse scan, a reduction peak centered at 1.78 V (vs RHE) was observed, indicating the deintercalation of sulfate anions (SO_4^{2-}) from the graphite layers. The second and third CV scans showed decreased onset potential and increased current for the overall oxidation reactions relative to the first scan. We postulate that the enhanced oxidation reactions may be associated with the enlarged surface area of the HOPG films due to irreversible expansion between graphene sheets. In addition, upon subsequent cycling, the anions can be more readily introduced to the edge of the film since the edge layer was expanded by the initially intercalated anions and subsequent gas evolution reactions. For 1 M H_3PO_4, the CV scans in the potential range of 1–2.0 V (vs RHE)

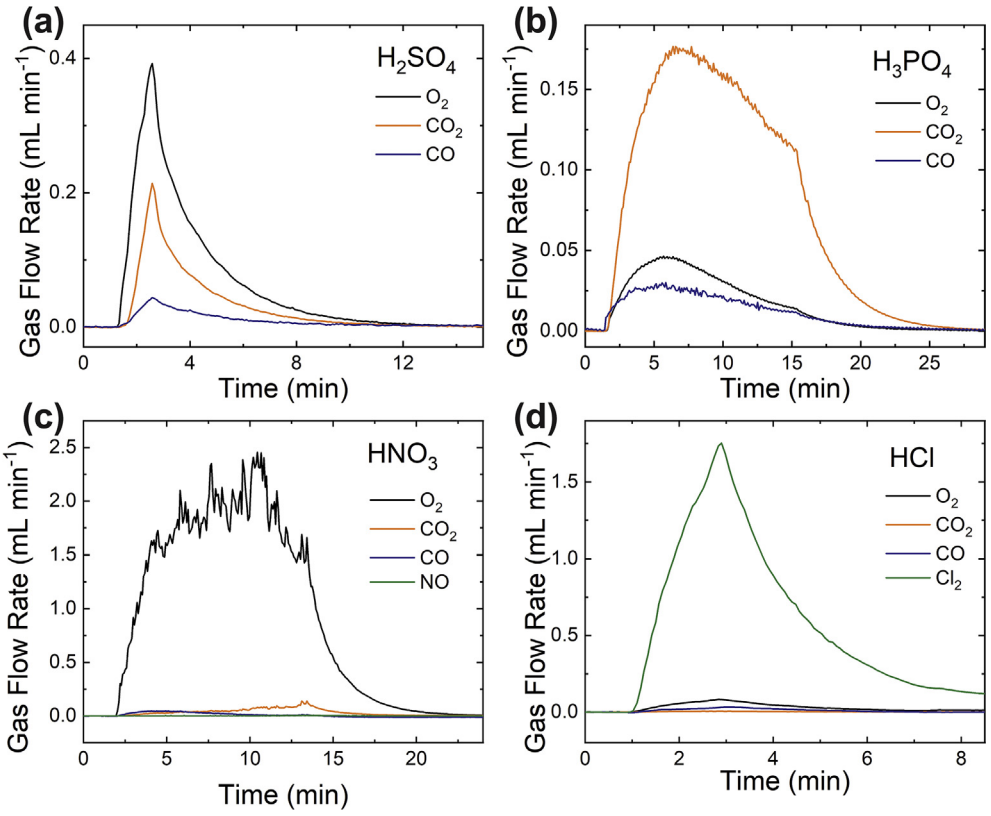

Fig. 3. Gas composition profiles over time obtained by in-situ gas analysis during the electrochemical exfoliation of HOPG foils by applying a voltage of 10 V to the electrodes in different electrolytes: (a) 1 M H_2SO_4, (b) 1 M HNO_3, (c) 1 M H_3PO_4, and (d) 1 M HCl. Hydrogen (H_2) gas generated on the Pt wire was excluded from the analysis. (A colour version of this figure can be viewed online.)

showed no intercalation/deintercalation peaks but a gradual increase in oxidation current with increasing potential due to the water and carbon oxidation reactions. When increasing an upper potential limit up to 2.5 V (vs RHE), the first CV scan in 1 M H_3PO_4 displayed an oxidation wave with an onset potential of 2.0 V (vs RHE), indicating the anion intercalation reaction at higher potentials compared to SO_4^{2-} (Fig. 4b). The second oxidation wave was observed with an onset potential of 2.25 V (vs RHE) due to the continuous water oxidation and carbon corrosion reactions. Interestingly, the H_3PO_4 electrolyte showed no reduction (deintercalation) peak in the reverse scan, indicating the irreversible intercalation reaction. For 1 M HNO_3 electrolyte, the first CV scan exhibited a clear oxidation peak with an onset potential of 1.72 V (vs RHE) followed by several oxidation peaks. We postulate that the strong oxidation peaks during the first CV scan may be associated with a combination of irreversible intercalation reaction of anions into the graphite and the previously mentioned oxidation reactions of nitrate anion [105]. In addition, the second and third CV scans showed no oxidation peaks or plateaus, but a strong oxidation wave associated with the water and carbon oxidation reactions. In addition, no reduction peak in the reverse scan indicates the irreversible intercalation reaction. The lower onset potential of ~1.72 V for the intercalation reaction compared to other electrolytes (H_2SO_4, H_3PO_4) may be attributed to the relatively small size of the anion (NO_3^-). However, after the first insertion, the NO_3^- ions could not easily diffuse through the HOPG interlayer, hindering the sequential introduction of anions in the second and third cycles. A previous study investigated the intercalation behavior of HOPG with different electrolytes using in situ Raman spectroscopy [108]. The ratio of the E_{2g}' and E_{2g} bands for HOPG as a function of potential in various electrolytes showed that the relative order of electrolyte intercalation imitation is $HNO_3 > H_2SO_4 > H_3PO_4$ [108], which is in good agreement with the trend of the intercalation onset potential of the CV scan results.

Using 1 M HCl as the electrolyte, almost identical CV shape was obtained from three repeated scans, as shown in Fig. 4d. The CV scans showed only a strong oxidation wave with an onset potential of ~1.7 V (vs RHE) without any plateaus or peaks. It is important to mention that the strong oxidation is not mainly due to oxidation of water or carbon, but mainly to oxidation of Cl^- ions. The in-situ gas analysis confirms the generation of chlorine gas during the CV scan (Fig. S10). Thus, in the case of the HCl electrolyte, most of the charges were consumed for the oxidation of Cl^-, resulting in failure of electrochemical exfoliation of HOPG (Fig. 1b). A previous study on graphite intercalation compounds also reported the reversible intercalation and deintercalation behavior of H_2SO_4 into natural graphite [107]. On the other hand, for H_3PO_4, HNO_3 and HCl, the anodic current flow does not produce any cathodic peak [107] which are consistent with our CV scan results. In addition, a recent study reported the electrochemical exfoliation of graphite foil into graphene in a dilute NaCl with sufficient exfoliation time of 60 min and continuous sonication in DMF for 3 h [109]. Interestingly, only 0.05 M concentration exhibited the exfoliation process of graphite foil, whereas other concentration conditions such as 0.01 M and 0.10 M did not show the exfoliation process [109]. The results suggest that there are subtle electrolyte conditions that enable the intercalation of Cl^- into the graphite. This topic is also interesting for future research.

To understand the intercalation and exfoliation behavior of graphite depending on the anionic species, we employ the DFT

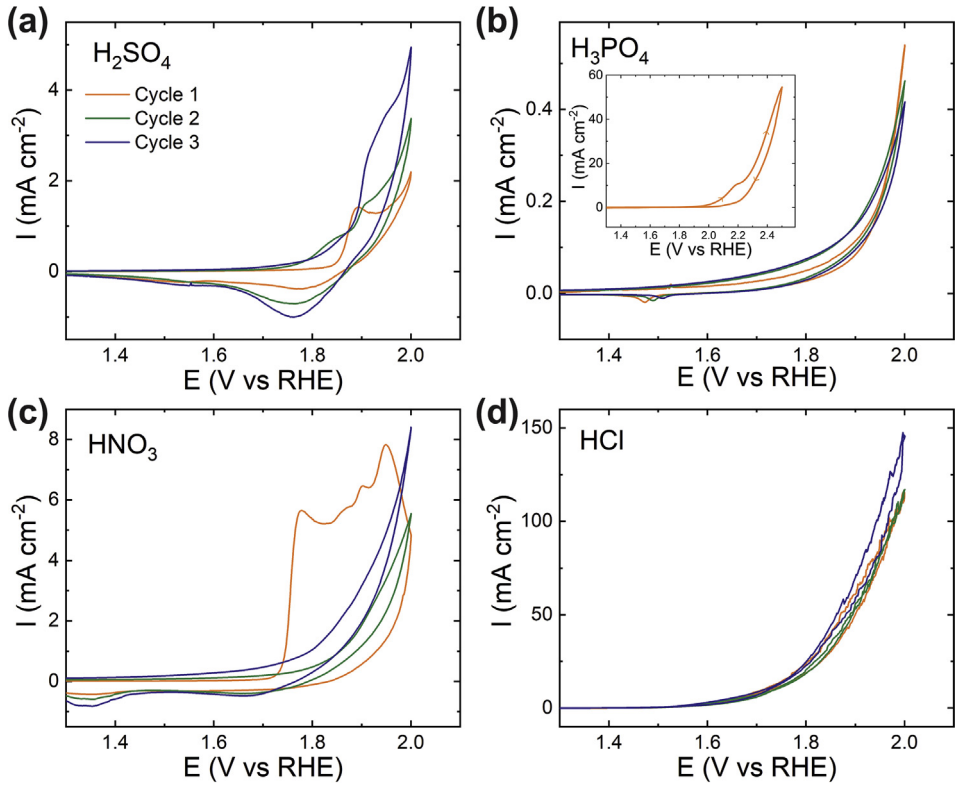

Fig. 4. Cyclic voltammograms obtained with different electrolytes: (a) 1 M H_2SO_4, (b) 1 M H_3PO_4, (c) 1 M HNO_3, and (d) 1 M HCl. The HOPG film, the Pt rod, and the reversible hydrogen electrode (RHE) were used as a working, a counter, and a reference electrode, respectively. Three consecutive cycles were carried out in the potential range of 1–2.0 V (vs RHE) for the electrolytes of H_2SO_4, HNO_3, and HCl, but 1–2.5 V (vs RHE) for H_3PO_4. (A colour version of this figure can be viewed online.)

computation modeling. Fig. 5a shows the optimized binding configurations of anionic species between graphene layers that produce different degree of separation according to the adopted ion species, where 7.116 Å, 7.402 Å, 5.545 Å, and 4.603 Å for the SO_4, H_2PO_4, NO_3, and Cl ions, respectively. These separation distances are greater than the graphite layer graphite (3.35 Å) [110,111], indicating that the intercalation of anions into the graphite leads the expansion of the graphite along the c-axis. The higher intercalation potential in H_2PO_4 (Fig. 4b) may be due to the larger separation distance, which can require a larger electromotive force for insertion. However, the separation distance trend cannot explain the high exfoliation efficiency of H_2SO_4. To further understand the exfoliation tendency, the binding energy of each ion on graphene was evaluated based on the optimized binding configuration for energy minimized ion-graphene structure by the following equation (2):

$$E_{binding} = E_{total} - 2E_{GR} - E_{Ion} + \frac{n}{2}E_{H_2} \quad (2)$$

where the E_{total}, E_{GR}, E_{ion}, and E_{H_2} are the energies of the total system, graphene single layer, ion molecule, and H_2 molecule, respectively. Fig. 5b plots the calculated binding energy of ionic species. It is interesting to note that the SO_4 ion has the highest repulsive binding energy (1.687 V nm^{-2}) compared to those of other anions (0.911 eV nm^{-2} for H_2PO_4, 0.402 eV nm^{-2} for NO_3, 0.551 ev nm^{-2} for Cl). We postulate that such repulsive interaction between SO_4 ion and graphene sheet is the origin of a reversible intercalation reaction during the CV cycles (Fig. 4a). The SO_4 ions with the highest repulsive binding energy can freely diffuse

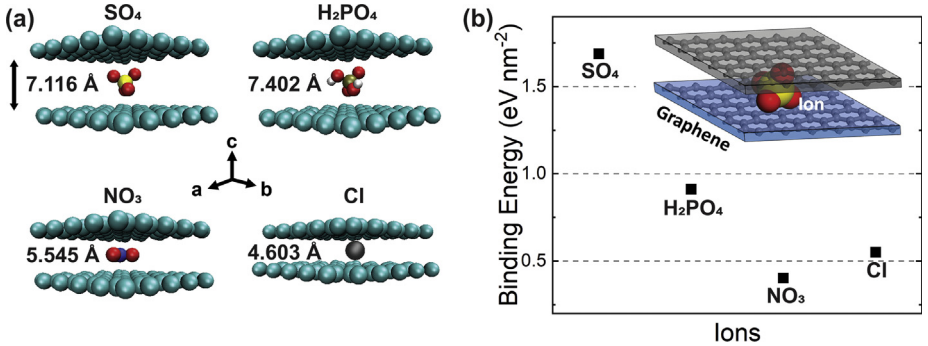

Fig. 5. (a) Inter-layer distances and binding configurations for energy minimized ion-graphene structures and (b) the corresponding binding energies of the four anions. Positive binding energy indicates a repulsive interaction, where the SO_4 shows the highest repulsive binding state. (A colour version of this figure can be viewed online.)

between the graphene layers, while other anions with higher binding energy have limited diffusion into the graphite layer. The high binding energy of H_2PO_4 and NO_3 may give rise to the irreversible intercalation behavior (no deintercalation peak) in their CV scans for 1 M H_3PO_4 and HNO_3 (Fig. 4b and c). Thus, we attribute the high exfoliation efficiency of sulfate ion to the facilitated diffusion of SO_4^{2-} ions between graphene layers. The diffusion of SO_4^{2-} ions can be accompanied by the diffusion of water molecules by hydrogen bonding through the expanded layer spacing. Subsequently, the diffused water molecules are oxidized to generate oxygen gas between the graphene layers, which can irreversibly expand and eventually exfoliate graphite into graphene. However, other electrolyte systems have several limitations for the effective exfoliation of graphite. First, the H_3PO_4 electrolyte requires a higher potential for the intercalation reaction of the anion, thus causing severe oxidation of the graphene products. The HNO_3 electrolyte with higher attractive binding energy has limitations on the diffusion of anions into the bulk of graphite. Thus, gas evolution reactions may mostly occur at the surface or the edge region of the graphite, resulting in small dimensions of the graphene products. Finally, for the HCl electrolyte, the oxidation of Cl^- ions prevents the intercalation reaction, exhibiting no exfoliation process of graphite.

To investigate the effect of electrolyte concentration on the electrochemical exfoliation, we further conducted CV with different concentrations of H_2SO_4 at 0.1, 1, and 4 M. As shown in Fig. 6a, the onset potentials of the oxidation wave gradually decreased from 1.9 to 1.6 V (vs RHE) as the concentration increased from 0.1 to 4 M. In addition, increasing the concentration of H_2SO_4 significantly increased overall oxidation current associated with the intercalation, indicating that the presence of more anions in the electrolyte could promote the anion intercalation reaction into the graphite layer. The chemical compositions of the graphene products in 0.1 M and 4 M were examined by XPS analysis (Fig. 6b and c). The graphene product obtained in 4 M H_2SO_4 contained higher amounts of sp^3 carbon and oxygen functional groups than those of 0.1 M and 1.0 M (Please see Fig. 2a). In the graphene product with 4 M H_2SO_4, the increased portions of sp^3 carbon and oxygen functional groups can be correlated with the increased amount of CO_2 generated during the electrochemical exfoliation process (The inset figure in Fig. 6c). Such a severe oxidation process with high concentrations of H_2SO_4 may facilitate the anion intercalation through accelerated oxidation of the edge carbon of HOPG. These results also suggest that the electrolyte concentration should be optimized to produce graphene with lower defect sites.

4. Conclusions

In summary, we have suggested direct evidence that effective intercalation of anion and subsequent water oxidation is a key enabling step for the efficient exfoliation of graphite into graphene. In-situ gas analysis revealed the generation of carbon dioxide (CO_2), carbon monoxide (CO), and oxygen (O_2) during the electrochemical exfoliation of graphite in dilute aqueous acids. Oxygen was the main gaseous product of sulfuric acid with the highest exfoliation efficiency, indicating that oxygen gas generated from water oxidation is essential for exfoliating graphite. Therefore, efficient delivery of water molecules into the bulk graphite structure is the key for the efficient exfoliation. The CV scans showed that only sulfate anions have reversible intercalation/deintercalation behavior, suggesting the facilitated diffusion of sulfate anions from the graphite surface into the bulk graphite structure. The calculated binding energy between sulfate anion to the graphene layer is the highest among other listed anions, which indicates that the sulfate anion is an efficient carrier of water molecules into the bulk graphite structure. This work, therefore, establishes the roles of anion intercalation and gas evolution for the anodic exfoliation of graphite into graphene. The results underscore the importance of understanding and controlling the interactions between electrolyte ion and 2D layered materials for the electrochemical exfoliation process.

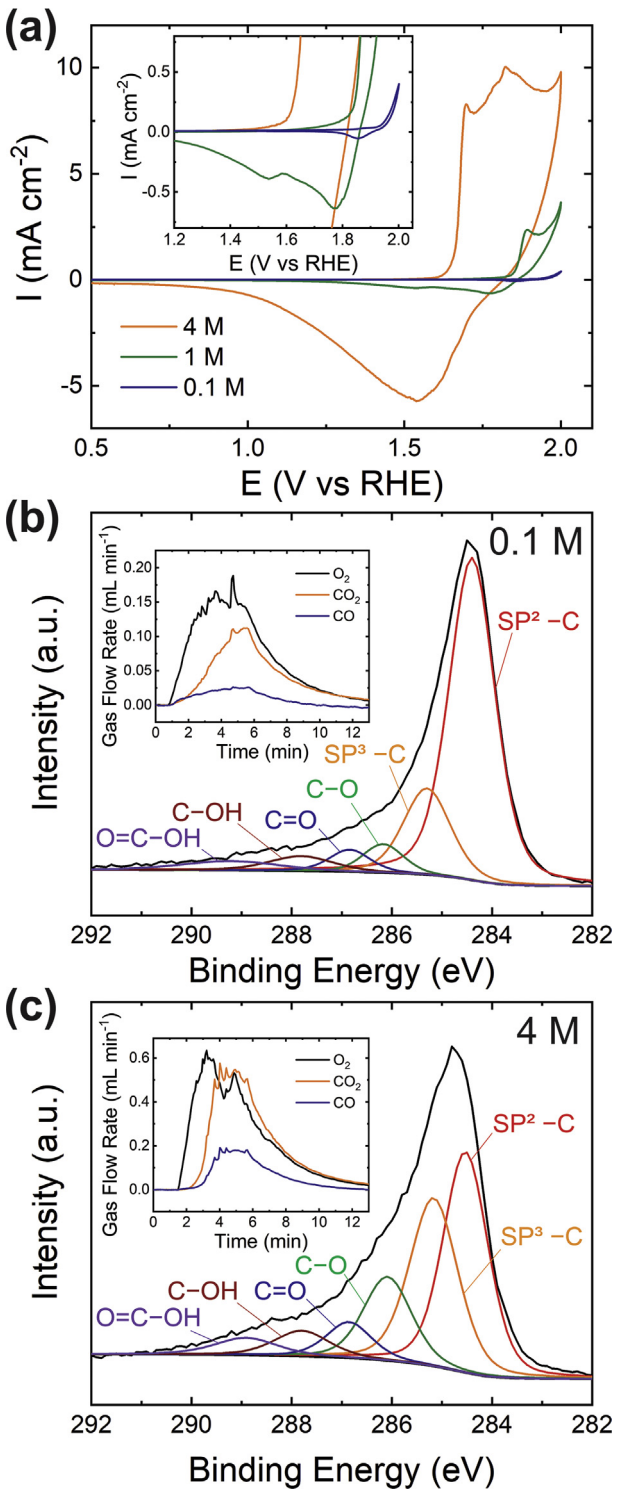

Fig. 6. (a) First CV scan of the HOPG electrodes in 0.1 M, 1 M, and 4 M H_2SO_4 at a scan rate of 1 mV/s. XPS high-resolution C1s spectrum of graphene products obtained in (b) 0.1 M H_2SO_4 and (c) 4 M H_2SO_4 (inset shows mass spectrum during the electrochemical exfoliation). (A colour version of this figure can be viewed online.)

CRediT authorship contribution statement

Hoyoung Lee: Conceptualization, Methodology, Validation, Formal analysis, Investigation, Data curation, Writing - original draft, Writing - review & editing, Visualization. **Ji Il Choi:** Methodology, Writing - original draft. **Jinho Park:** Methodology, Writing - original draft. **Seung Soon Jang:** Resources, Writing - original draft. **Seung Woo Lee:** Conceptualization, Methodology, Writing - original draft, Writing - review & editing, Visualization, Supervision, Project administration, Funding acquisition.

Declaration of competing interest

There are no conflicts to declare.

Acknowledgements

This material is based upon work supported by the National Science Foundation under Grant No.1751693. This work was performed in part at the Georgia Tech Institute for Electronics and Nanotechnology, a member of the National Nanotechnology Infrastructure Network, which is supported by the National Science Foundation.

Appendix B. Supplementary data

Supplementary data to this article can be found online at https://doi.org/10.1016/j.carbon.2020.06.044.

References

[1] K.S. Novoselov, A.K. Geim, S.V. Morozov, D. Jiang, Y. Zhang, S.V. Dubonos, et al., Science 306 (2004) 666–669.
[2] K.I. Bolotin, K.J. Sikes, Z. Jiang, M. Klima, G. Fudenberg, J. Hone, et al., Solid State Commun. 146 (2008) 351–355.
[3] J. Stangl, V. Holý, G. Bauer, Rev. Mod. Phys. 76 (2004) 725–783.
[4] A.K. Geim, K.S. Novoselov, The Rise of Graphene, Nanoscience and Technology, Co-Published with Macmillan Publishers Ltd, UK, 2009, pp. 11–19.
[5] C. Lee, X. Wei, J.W. Kysar, J. Hone, Science 321 (2008) 385.
[6] S. Park, R.S. Ruoff, Nat. Nanotechnol. 4 (2009) 217–224.
[7] A.A. Balandin, S. Ghosh, W. Bao, I. Calizo, D. Teweldebrhan, F. Miao, et al., Nano Lett. 8 (2008) 902–907.
[8] S. Bae, H. Kim, Y. Lee, X. Xu, J.-S. Park, Y. Zheng, et al., Nat. Nanotechnol. 5 (2010) 574–578.
[9] T. Ramanathan, A.A. Abdala, S. Stankovich, D.A. Dikin, M. Herrera-Alonso, R.D. Piner, et al., Nat. Nanotechnol. 3 (2008) 327–331.
[10] S. Stankovich, D.A. Dikin, G.H.B. Dommett, K.M. Kohlhaas, E.J. Zimney, E.A. Stach, et al., Nature 442 (2006) 282–286.
[11] N. Liu, F. Luo, H. Wu, Y. Liu, C. Zhang, J. Chen, Adv. Funct. Mater. 18 (2008) 1518–1525.
[12] F. Chen, J. Ying, Y. Wang, S. Du, Z. Liu, Q. Huang, Carbon 96 (2016) 836–842.
[13] V.B. Mohan, K. Jayaraman, D. Bhattacharyya, Int. J. Soc. Netw. Min. 7 (2016) 179–201.
[14] T. Kuilla, S. Bhadra, D. Yao, N.H. Kim, S. Bose, J.H. Lee, Prog. Polym. Sci. 35 (2010) 1350–1375.
[15] S. Stankovich, R.D. Piner, S.T. Nguyen, R.S. Ruoff, Carbon 44 (2006) 3342–3347.
[16] P. Avouris, Nano Lett. 10 (2010) 4285–4294.
[17] Q. He, S. Wu, Z. Yin, H. Zhang, Chem. Sci. 3 (2012) 1764–1772.
[18] E.-C. Cho, J.-H. Huang, C.-P. Li, C.-W. Chang-Jian, K.-C. Lee, Y.-S. Hsiao, et al., Carbon 102 (2016) 66–73.
[19] M.D. Stoller, S. Park, Y. Zhu, J. An, R.S. Ruoff, Nano Lett. 8 (2008) 3498–3502.
[20] Y. Sun, Q. Wu, G. Shi, Energy Environ. Sci. 4 (2011) 1113–1132.
[21] M. Pumera, Energy Environ. Sci. 4 (2011) 668–674.
[22] P.V. Kamat, J. Phys. Chem. Lett. 2 (2011) 242–251.
[23] L. Dai, Acc. Chem. Res. 46 (2013) 31–42.
[24] L.L. Zhang, X.S. Zhao, Chem. Soc. Rev. 38 (2009) 2520–2531.
[25] E. Dervishi, Z. Li, F. Watanabe, A. Biswas, Y. Xu, A.R. Biris, et al., Chem. Commun. (2009) 4061–4063.
[26] S. Bae, H. Kim, Y. Lee, X. Xu, J.-S. Park, Y. Zheng, et al., Nat. Nanotechnol. 5 (2010) 574–578.
[27] K.V. Emtsev, A. Bostwick, K. Horn, J. Jobst, G.L. Kellogg, L. Ley, et al., Nat. Mater. 8 (2009) 203–207.
[28] V. Eswaraiah, S.S. Jyothirmayee Aravind, S. Ramaprabhu, J. Mater. Chem. 21 (2011) 6800–6803.
[29] M. Buzaglo, E. Ruse, I. Levy, R. Nadiv, G. Reuveni, M. Shtein, et al., Chem. Mater. 29 (2017) 9998–10006.
[30] L. Liu, Z. Xiong, D. Hu, G. Wu, P. Chen, Chem. Commun. 49 (2013) 7890–7892.
[31] K. Parvez, R. Li, S.R. Puniredd, Y. Hernandez, F. Hinkel, S. Wang, et al., ACS Nano 7 (2013) 3598–3606.
[32] M. Lotya, Y. Hernandez, P.J. King, R.J. Smith, V. Nicolosi, L.S. Karlsson, et al., J. Am. Chem. Soc. 131 (2009) 3611–3620.
[33] J. Wang, K.K. Manga, Q. Bao, K.P. Loh, J. Am. Chem. Soc. 133 (2011) 8888–8891.
[34] D. Li, M.B. Müller, S. Gilje, R.B. Kaner, G.G. Wallace, Nat. Nanotechnol. 3 (2008) 101–105.
[35] K.S. Novoselov, A.K. Geim, S.V. Morozov, D. Jiang, Y. Zhang, S.V. Dubonos, et al., Science 306 (2004) 666–669.
[36] J.N. Coleman, Acc. Chem. Res. 46 (2013) 14–22.
[37] M.J. McAllister, J.-L. Li, D.H. Adamson, H.C. Schniepp, A.A. Abdala, J. Liu, et al., Chem. Mater. 19 (2007) 4396–4404.
[38] D.C. Marcano, D.V. Kosynkin, J.M. Berlin, A. Sinitskii, Z. Sun, A. Slesarev, et al., ACS Nano 4 (2010) 4806–4814.
[39] W.S. Hummers, R.E. Offeman, J. Am. Chem. Soc. 80 (1958), 1339-1339.
[40] D.R. Dreyer, S. Park, C.W. Bielawski, R.S. Ruoff, Chem. Soc. Rev. 39 (2010) 228–240.
[41] S. Pei, H.-M. Cheng, Carbon 50 (2012) 3210–3228.
[42] S. Pang, H.N. Tsao, X. Feng, K. Müllen, Adv. Mater. 21 (2009) 3488–3491.
[43] S. Park, J. An, J.R. Potts, A. Velamakanni, S. Murali, R.S. Ruoff, Carbon 49 (2011) 3019–3023.
[44] H.-J. Shin, K.K. Kim, A. Benayad, S.-M. Yoon, H.K. Park, I.-S. Jung, et al., Adv. Funct. Mater. 19 (2009) 1987–1992.
[45] I.K. Moon, J. Lee, R.S. Ruoff, H. Lee, Nat. Commun. 1 (2010) 73.
[46] J.O. Besenhard, Carbon 14 (1976) 111–115.
[47] L.B. Ebert, Annu. Rev. Mater. Sci. 6 (1976) 181–211.
[48] J.E. Fischer, T.E. Thompson, Phys. Today 31 (1978) 36–&.
[49] T. Ohzuku, Y. Iwakoshi, K. Sawai, J. Electrochem. Soc. 140 (1993) 2490–2498.
[50] M.S. Dresselhaus, G. Dresselhaus, Adv. Phys. 51 (2002) 1–186.
[51] T. Nakajima, K. Nakane, M. Kawaguchi, N. Watanabe, Carbon 25 (1987) 685–689.
[52] F. Beck, H. Krohn, E. Zimmer, Electrochim. Acta 31 (1986) 371–376.
[53] M.S. Dresselhaus, G. Dresselhaus, Adv. Phys. 30 (1981) 139–326.
[54] T. Inoshita, K. Nakao, H. Kamimura, J. Phys. Soc. Jpn. 43 (1977) 1237–1243.
[55] M.S. Dresselhaus, G. Dresselhaus, J.E. Fischer, Phys. Rev. B 15 (1977) 3180–3192.
[56] K.W. Hathcock, J.C. Brumfield, C.A. Goss, E.A. Irene, R.W. Murray, Anal. Chem. 67 (1995) 2201–2206.
[57] D. Alliata, P. Häring, O. Haas, R. Kötz, H. Siegenthaler, Electrochem. Commun. 1 (1999) 5–9.
[58] D. Alliata, R. Kötz, O. Haas, H. Siegenthaler, Langmuir 15 (1999) 8483–8489.
[59] P. Simon, Y. Gogotsi, Acc. Chem. Res. 46 (2013) 1094–1103.
[60] C. Gómez-Navarro, M. Burghard, K. Kern, Nano Lett. 8 (2008) 2045–2049.
[61] Z.-S. Wu, W. Ren, L. Gao, J. Zhao, Z. Chen, B. Liu, et al., ACS Nano 3 (2009) 411–417.
[62] M.A. Worsley, P.J. Pauzauskie, T.Y. Olson, J. Biener, J.H. Satcher, T.F. Baumann, J. Am. Chem. Soc. 132 (2010) 14067–14069.
[63] P. Yu, S.E. Lowe, G.P. Simon, Y.L. Zhong, Curr. Opin. Colloid Interface Sci. 20 (2015) 329–338.
[64] Y.R. Leroux, J.-F. Bergamini, S. Ababou, J.-C. Le Breton, P. Hapiot, J. Electroanal. Chem. 753 (2015) 42–46.
[65] W. Wei, G. Wang, S. Yang, X. Feng, K. Müllen, J. Am. Chem. Soc. 137 (2015) 5576–5581.
[66] A.M. Abdelkader, I.A. Kinloch, R.A.W. Dryfe, ACS Appl. Mater. Interfaces 6 (2014) 1632–1639.
[67] K. Parvez, Z.-S. Wu, R. Li, X. Liu, R. Graf, X. Feng, et al., J. Am. Chem. Soc. 136 (2014) 6083–6091.
[68] D. Wei, L. Grande, V. Chundi, R. White, C. Bower, P. Andrew, et al., Chem. Commun. 48 (2012) 1239–1241.
[69] C.-Y. Su, A.-Y. Lu, Y. Xu, F.-R. Chen, A.N. Khlobystov, L.-J. Li, ACS Nano 5 (2011) 2332–2339.
[70] J. Liu, C.K. Poh, D. Zhan, L. Lai, S.H. Lim, L. Wang, et al., Nano Energy 2 (2013) 377–386.
[71] H. Xuhua, L. Senlin, Q. Zhiqiang, Z. Wei, Y. Wei, F. Yanyan, Nanotechnology 26 (2015) 105602.
[72] J. Lu, J.-x. Yang, J. Wang, A. Lim, S. Wang, K.P. Loh, ACS Nano 3 (2009) 2367–2375.
[73] K.S. Rao, J. Senthilnathan, Y.-F. Liu, M. Yoshimura, Sci. Rep. 4 (2014).
[74] K. Parvez, S. Yang, X. Feng, K. Müllen, Synth. Met. 210 (2015) 123–132.
[75] J.M. Munuera, J.I. Paredes, S. Villar-Rodil, M. Ayan-Varela, A. Martinez-Alonso, J.M.D. Tascon, Nanoscale 8 (2016) 2982–2998.
[76] A. Ejigu, I.A. Kinloch, R.A.W. Dryfe, ACS Appl. Mater. Interfaces 9 (2017) 710–721.
[77] H.C. Tao, Y.Q. Zhang, Y.N. Gao, Z.Y. Sun, C. Yan, J. Texter, Phys. Chem. Chem. Phys. 19 (2017) 921–960.
[78] S. Yang, A.G. Ricciardulli, S. Liu, R. Dong, M.R. Lohe, A. Becker, et al., Angew. Chem. Int. Ed. 56 (2017) 6669–6675.
[79] A.M. Abdelkader, A.J. Cooper, R.A.W. Dryfe, I.A. Kinloch, Nanoscale 7 (2015) 6944–6956.
[80] S. Yang, S. Brüller, Z.-S. Wu, Z. Liu, K. Parvez, R. Dong, et al., J. Am. Chem. Soc.

137 (2015) 13927–13932.
[81] C.-H. Chen, S.-W. Yang, M.-C. Chuang, W.-Y. Woon, C.-Y. Su, Nanoscale 7 (2015) 15362–15373.
[82] J.M. Munuera, J.I. Paredes, S. Villar-Rodil, A. Castro-Muñiz, A. Martínez-Alonso, J.M.D. Tascón, Applied Materials Today 11 (2018) 246–254.
[83] A.J. Cooper, N.R. Wilson, I.A. Kinloch, R.A.W. Dryfe, Carbon 66 (2014) 340–350.
[84] Y.L. Zhong, T.M. Swager, J. Am. Chem. Soc. 134 (2012) 17896–17899.
[85] F. Beck, J. Jiang, H. Krohn, J. Electroanal. Chem. 389 (1995) 161–165.
[86] Y. Liu, B.V. Merinov, W.A. Goddard, Proc. Natl. Acad. Sci. Unit. States Am. 113 (2016) 3735–3739.
[87] G. Kresse, J. Hafner, Phys. Rev. B 47 (1993) 558–561.
[88] G. Kresse, J. Furthmüller, Phys. Rev. B 54 (1996) 11169–11186.
[89] J.P. Perdew, K. Burke, M. Ernzerhof, Phys. Rev. Lett. 77 (1996) 3865–3868.
[90] S. Grimme, J. Antony, S. Ehrlich, H. Krieg, J. Chem. Phys. 132 (2010) 154104.
[91] H.J. Monkhorst, J.D. Pack, Phys. Rev. B 13 (1976) 5188–5192.
[92] Y. Setsuhara, K. Cho, M. Shiratani, M. Sekine, M. Hori, Thin Solid Films 518 (2010) 6492–6495.
[93] S.W. Lee, B.-S. Kim, S. Chen, Y. Shao-Horn, P.T. Hammond, J. Am. Chem. Soc. 131 (2009) 671–679.
[94] B. Cord, J. Yang, H. Duan, D.C. Joy, J. Klingfus, K.K. Berggren, J. Vac. Sci. Technol. B: Microelectronics and Nanometer Structures Processing, Measurement, and Phenomena 27 (2009) 2616–2621.
[95] B. Schnyder, D. Alliata, R. Kötz, H. Siegenthaler, Appl. Surf. Sci. 173 (2001) 221–232.
[96] Y. Yi, G. Weinberg, M. Prenzel, M. Greiner, S. Heumann, S. Becker, et al., Catal. Today 295 (2017) 32–40.
[97] T.Y. Leung, W.F. Man, P.K. Lim, W.C. Chan, F. Gaspari, S. Zukotynski, J. Non-Cryst. Solids 254 (1999) 156–160.
[98] R.P. Vidano, D.B. Fischbach, L.J. Willis, T.M. Loehr, Solid State Commun. 39 (1981) 341–344.
[99] J.-B. Wu, M.-L. Lin, X. Cong, H.-N. Liu, P.-H. Tan, Chem. Soc. Rev. 47 (2018) 1822–1873.
[100] A.C. Ferrari, Solid State Commun. 143 (2007) 47–57.
[101] R. Vidano, D.B. Fischbach, J. Am. Ceram. Soc. 61 (1978) 13–17.
[102] B. Krauss, T. Lohmann, D.H. Chae, M. Haluska, K. von Klitzing, J.H. Smet, Phys. Rev. B 79 (2009) 165428.
[103] F. Zhao, J. Liu, X. Huang, X. Zou, G. Lu, P. Sun, et al., ACS Nano 6 (2012) 3027–3033.
[104] S.A. Shafiee, J. Aarons, H.H. Hamzah, J. Electrochem. Soc. 165 (2018) H785–H798.
[105] T.L. Broder, D.S. Silvester, L. Aldous, C. Hardacre, A. Crossley, R.G. Compton, New J. Chem. 31 (2007) 966–972.
[106] B.J. Finlayson-Pitts, L.M. Wingen, A.L. Sumner, D. Syomin, K.A. Ramazan, Phys. Chem. Chem. Phys. 5 (2003) 223–242.
[107] F. Beck, H. Junge, H. Krohn, Electrochim. Acta 26 (1981) 799–809.
[108] D.C. Alsmeyer, R.L. McCreery, Anal. Chem. 64 (1992) 1528–1533.
[109] J.M. Munuera, J.I. Paredes, M. Enterría, A. Pagán, S. Villar-Rodil, M.F.R. Pereira, et al., ACS Appl. Mater. Interfaces 9 (2017) 24085–24099.
[110] J.D. Bernal, W.L. Bragg, Proc. R. Soc. Lond. - Ser. A Contain. Pap. a Math. Phys. Character 106 (1924) 749–773.
[111] D.D.L. Chung, J. Mater. Sci. 37 (2002) 1475–1489.

Supporting Information

Role of Anions on Electrochemical Exfoliation of Graphite in-to Graphene in Aqueous Acids

Hoyoung Lee,[a] Ji Il Choi,[b] Jinho Park,[a] Seung Soon Jang,[b,*] and Seung Woo Lee[a,*]

[a]*George W. Woodruff School of Mechanical Engineering, Georgia Institute of Technology, Atlanta, Georgia 30332, USA*

[b]*Computational NanoBio Technology Laboratory, School of Material Science and Engineering, Georgia Institute of Technology, Atlanta, GA 30332, USA.*

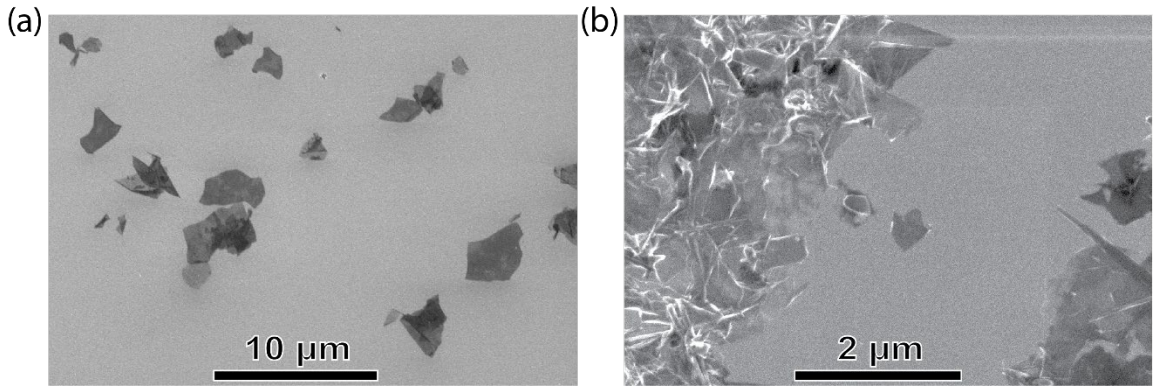

Fig. S1. (a and b) SEM images of the graphene product obtained from 1M HNO_3.

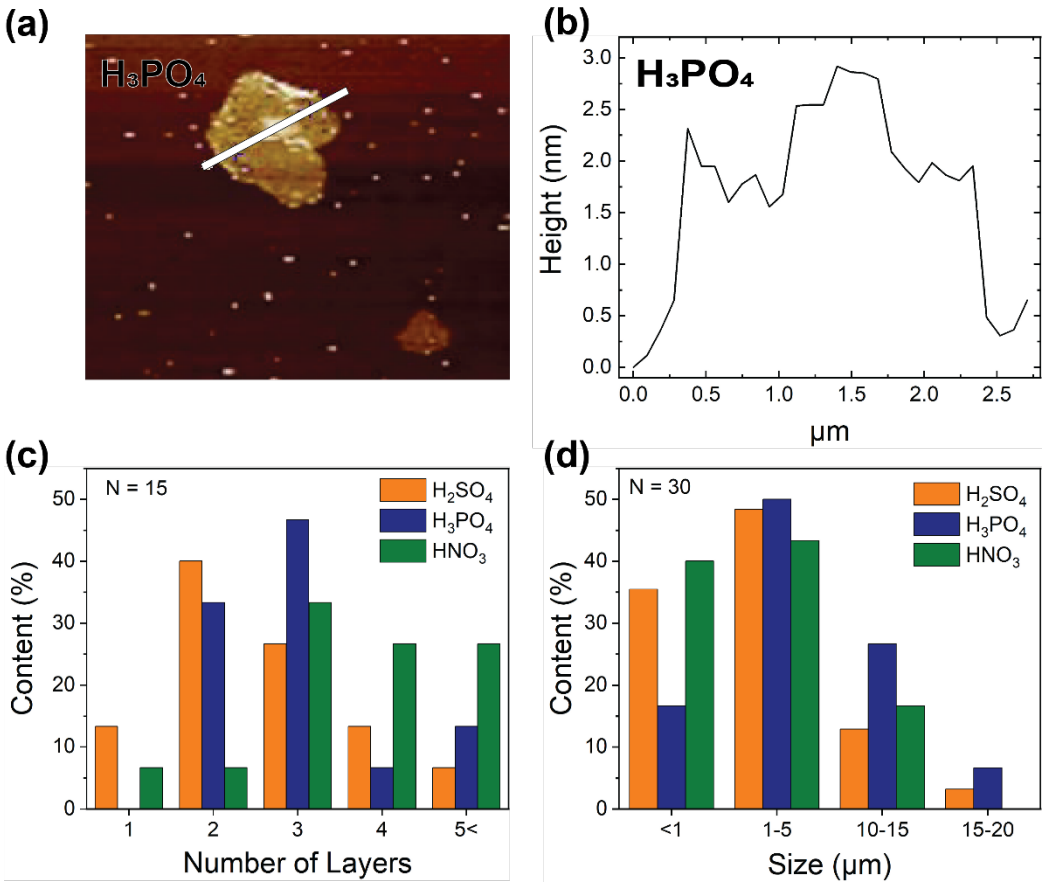

Fig. S2. (a) AFM image of electrochemically exfoliated graphene in 1M H3PO4 and (b) height profile. Statistical (c) number of layers and (d) flake size analysis of electrochemically exfoliated graphene in different electrolytes. N is the sample size.

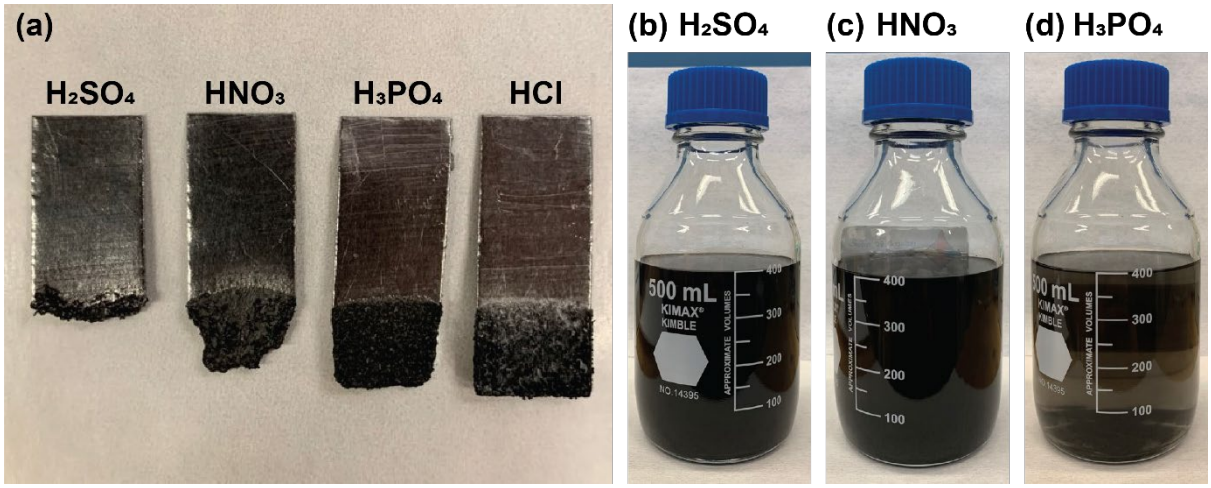

Fig. S3. (a) Picture of graphite foil after electrochemical exfoliation (10 V) in 0.1M of each electrolyte for 5 min. Photographs of exfoliated graphite particles from (b) 0.1M H_2SO_4, (c) 0.1M HNO_3, and (d) 0.1M H_3PO_4 in dimethyl formamide (DMF) solvent.

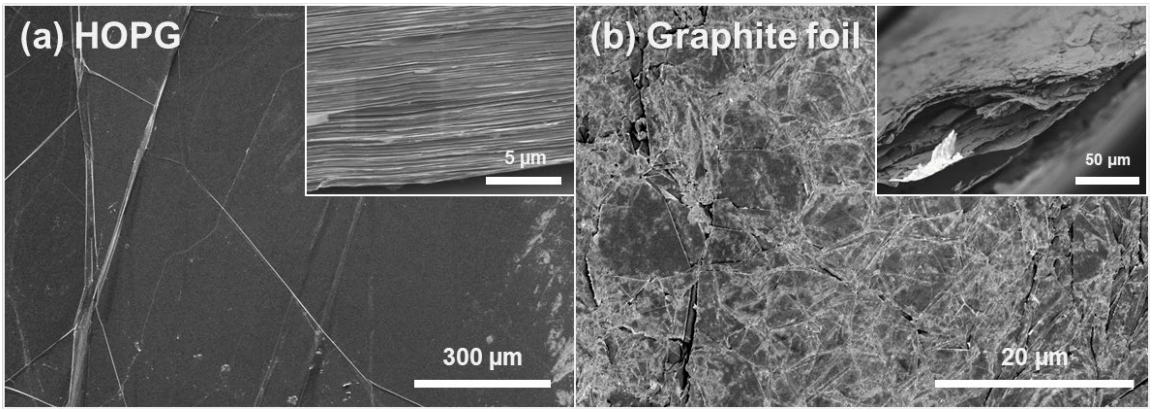

Fig. S4. SEM images of (a) HOPG and (b) graphite foil.

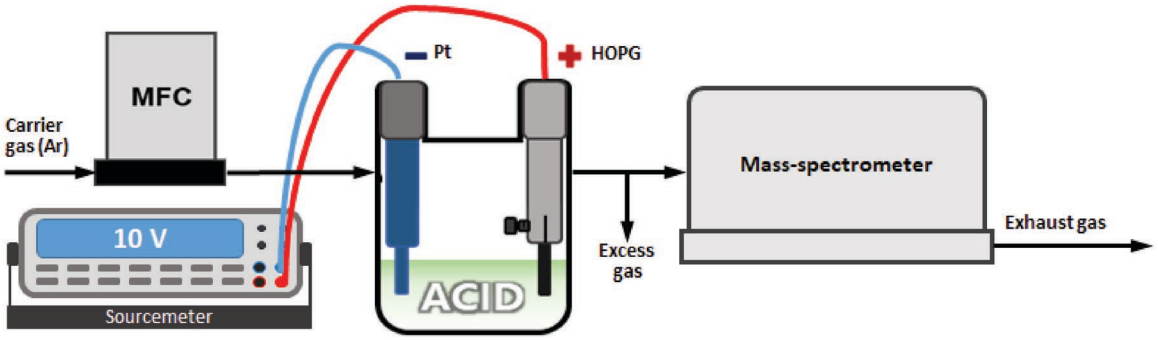

Fig. S5. Schematic illustration of in-situ mass spectroscopy set-up for the electrochemical exfoliation process.

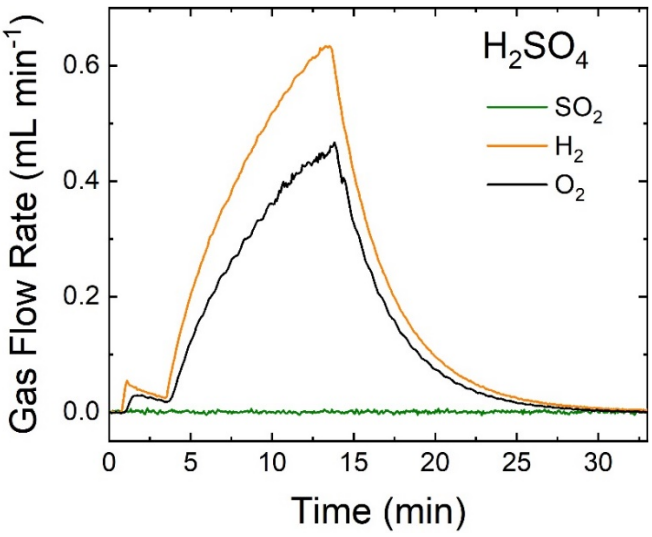

Fig. S6. Gas composition profiles over time obtained by in-situ gas analysis during the water electrolysis using an Au cathode and a Pt anode at 10 V in 1 M H_2SO_4.

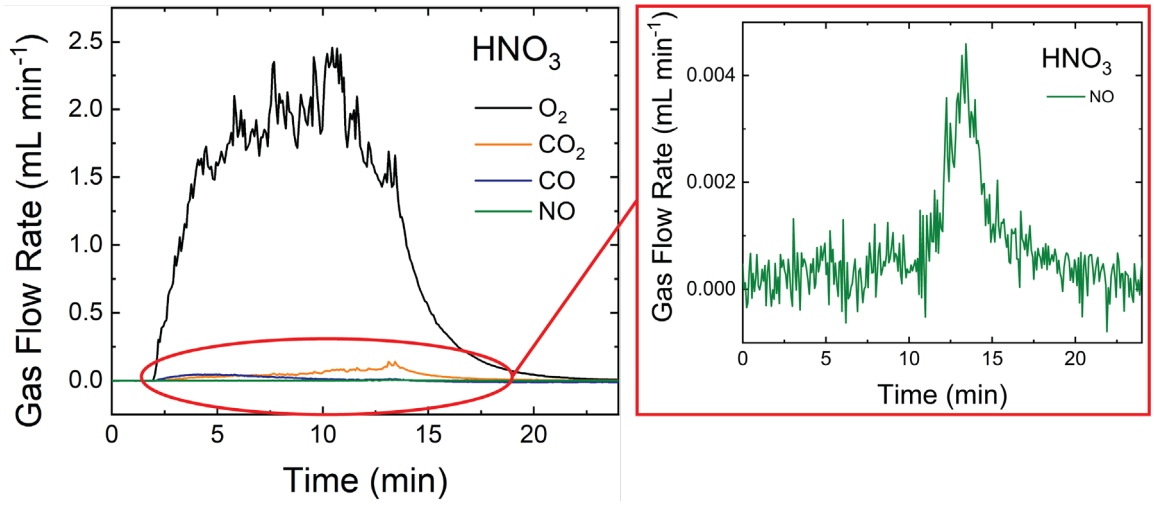

Fig. S7. NO gas generation during the electrochemical exfoliation of HOPG in 1M HNO_3.

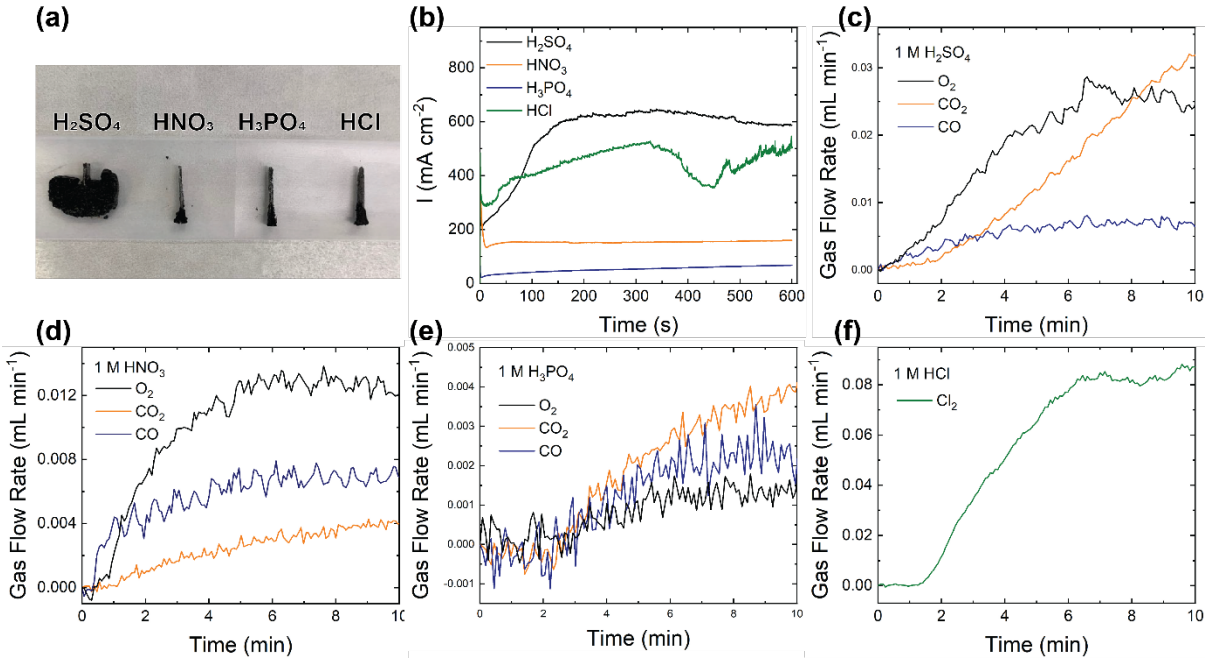

Fig. S8. (a) Digital images of HOPGs after potential holding of 2.4 V (vs RHE) for 10 min in different dilute acids. (b) I-t curve and (c-f) gas flow spectrum during the potential holding of 2.4 V (vs RHE) in 1M H_2SO_4, HNO_3, H_3PO_4, and HCl, respectively.

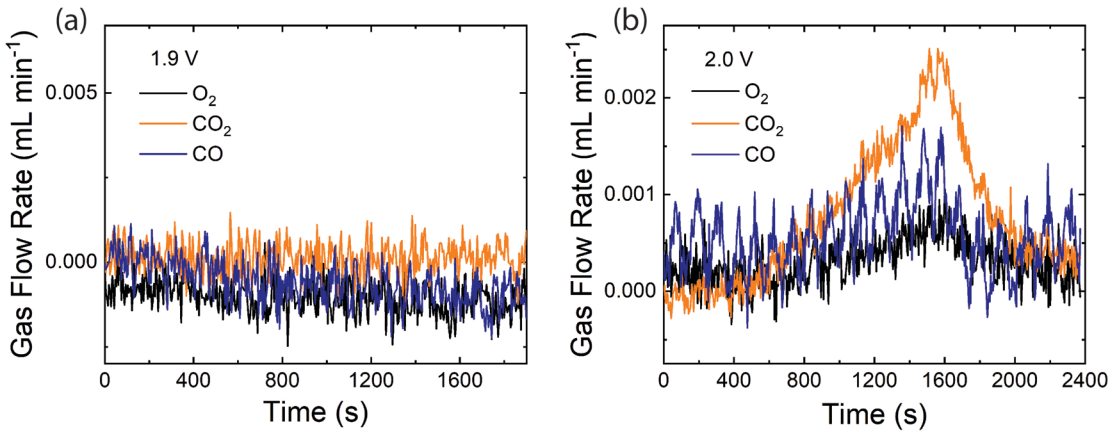

Fig. S9. Gas flow spectrum during the potential holding of (a) 1.9 V (vs RHE) and (b) 2.0 V (vs RHE) on HOPG for 30 min in 1M H_2SO_4.

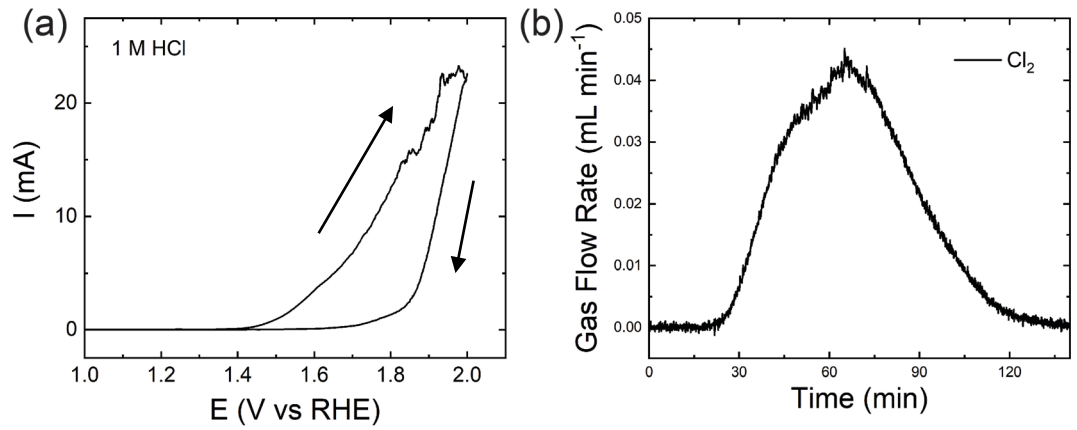

Fig. S10. (a) CV scan of HOPG in 1M HCl from 0 to 2 V (vs RHE) at a scan rate of 1 mV s^{-1}.

(b) Mass spectrum of during the CV scan.